See discussions, stats, and author profiles for this publication at: https://www.researchgate.net/publication/320963864

# Parameter Optimization Algorithm of a Discrete Energy-Averaged Model for Galfenol Alloys

	nce Paper · September 2017 /SMASIS2017-3906		
CITATIONS		READS	
0		7	
4 author	s, including:		
	Ismail Nas		Zhangxian Deng
	The Ohio State University		The Ohio State University
	1 PUBLICATION 0 CITATIONS		18 PUBLICATIONS 60 CITATIONS
	SEE PROFILE		SEE PROFILE

### SMASIS2017-3906

# PARAMETER OPTIMIZATION ALGORITHM OF A DISCRETE ENERGY-AVERAGED MODEL FOR GALFENOL ALLOYS

Ismail Nas, Zhangxian Deng, Suryarghya Chakrabarti<sup>1</sup>, Marcelo J. Dapino
Department of Mechanical and Aerospace Engineering, The Ohio State University
Columbus, Ohio 43210

#### ABSTRACT

An optimization algorithm is proposed to determine the parameters of a discrete energy-averaged (DEA) model for Galfenol alloys. A new numerical approximation approach for partial derivative expressions is developed, which improves computational speed of the DEA model by 61% relative to existing partial derivative expressions. Initial estimation of model parameters and a two-step optimization procedure, including anhysteresis and hysteresis steps, are performed to improve accuracy and efficiency of the algorithm. Initial estimation of certain material properties such as saturation magnetization, saturation magnetostriction, Young's modulus, and anisotropy energies can improve the convergence and enhance efficiency by 41% compared to the case where these parameters are not estimated. The two-step optimization improves efficiency by 28% while preserving accuracy compared to one-step optimization. Proposed algorithm is employed to find the material properties of Galfenol samples with different compositions and heat treatments. The trends obtained from these optimizations can guide future Galfenol modeling studies.

#### INTRODUCTION

Magnetostrictive materials deform when exposed to magnetic fields and undergo change in magnetization when stressed. Magnetostrictive iron-gallium alloys, also known as Galfenol, possess a unique combination of mechanical robustness and

possess a unique combination of mechanical robustness and

moderate magnetostriction. Galfenol can withstand bending, tensile, and torsional loads and can be machined, welded, or extruded into complex geometries. Thus it opens up avenues for three-dimensional (3D) functional, structural, and versatile magnetostrictive devices including energy harvesters [1,2,3,4], sensors [5,6,7,8,9], actuators [10,11,12,13,14], and mechanical dampers [15,16,17].

Implementing constitutive models of magnetostrictive materials in device-level modeling can be challenging. Finite element modeling has been implemented to that effect, both in 2D [18, 19, 20] and in 3D [21, 22, 23] frameworks. Lumped parameter approximations have also been implemented, including single degree of freedom [2, 24], and multiple degrees of freedom [25, 26, 27]. The constitutive models should have two essential characteristics: efficiency that allows for high computational speed and accuracy that describes the fully-coupled and nonlinear magnetostrictive behavior. Earlier works modeled magnetostrictive behavior using measurement-fitted polynomial [28, 29, 30] that can be easily differentiated and implemented. However, this procedure requires a different set of coefficients once the preload or bias magnetic field conditions change. The measurement-fitted polynomial only works for 1D cases, since the computational effort increases exponentially with respect to the dimension of spline functions.

Fully-coupled 3D modeling frameworks for magnetostrictive materials have been developed in previous studies following an energy-based approach, which was first introduced by Armstrong [31]. In this approach, the bulk behavior is defined as a weighted sum of the local response of each magnetic domain,

<sup>&</sup>lt;sup>1</sup>Currently affiliated with GE Global Research Center, Niskayuna, New York 12309

where the local response depends on the orientation of magnetic domains and the weights, also known as the volume fractions, are determined by an energy-based Boltzmann distribution. Atulasimha et al. [32] improved the model by tracking the evolution of volume fractions belonging to 98 magnetic moments, resulting in an improved accuracy of describing the behavior in  $\langle 110 \rangle$ -oriented single-crystal Galfenol. Taking advantage of cubic symmetric Galfenol, Evans and Dapino [33] developed a 3D nonlinear discrete energy-averaged (DEA) model and significantly improved model efficiency by reducing the possible magnetic moment orientations to six. The DEA model has been shown to be 100 times faster than previous energy weighting models with same level of accuracy.

The response of Galfenol varies significantly depending on its composition [34] and material processing techniques [35]. For example, increasing gallium content from 18.4% to 20.9% reduces the saturation magnetostriction but increases the stress range over which the material shows a stress-dependent susceptibility change [36]. Through stress-annealing [37], a tetragonal anisotropy can be introduced in Galfenol where the two  $\langle 100 \rangle$  easy directions parallel to the annaealing direction have a higher anisotropy energy than the remaining four orientations in the basal plane. This enables the alloy to exhibit maximum magnetostriction without pre-compression. In order to account for the material property variations in Galfenol transducer modeling, a universal algorithm which optimizes the constitutive model parameters is necessary for improving the applicability of the DEA model.

This paper aims at developing a systematic procedure to estimate the parameters of the DEA model for Galfenol and relating trends in model parameters to material compositions and heat treatments. Key elements of previously-defined DEA model are presented in the following section. A two-step optimization algorithm, including anhysteresis and hysteresis steps, and techniques to estimate material parameters are described in the procedure section. In the results section, the performance of the optimization algorithm is analyzed for an unannealed textured polycrystalline  $Fe_{81.6}Ga_{18.4}$  sample, and the algorithm is applied to several Galfenol samples with various gallium contents and heat treatments.

## DISCRETE ENERGY-AVERAGED CONSTITUTIVE MODEL

Models based on energy-weighted averaging employ statistical mechanics to calculate the bulk magnetization and strain of the material. Armstrong [31] calculated the macroscopic material response as an expected value of a large number of possible energy states, or domain orientations, with an energy-based probability density function. Due to the large computational effort involved in evaluating the expected values by solving 2D integrals numerically, a discrete version of the model was devel-

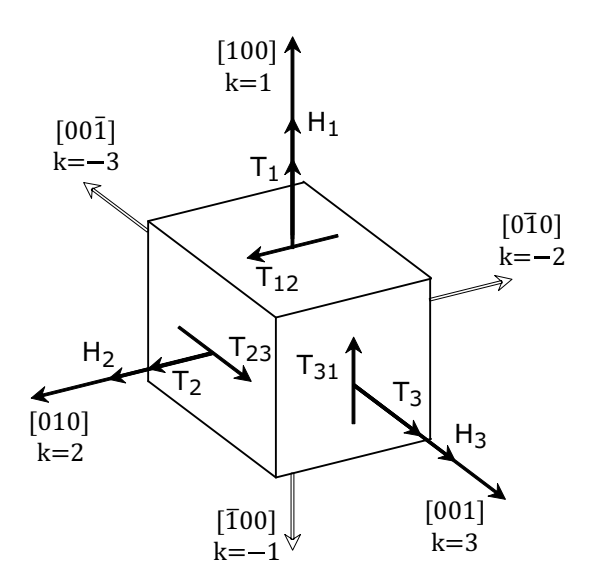


**FIGURE 1**. THE NOTATION USED IN THIS WORK TO NUMERATE THE EASY AXES.

oped [38]. The choice of possible domain orientations was restricted to the easy magnetization axes and the associated volume fractions were calculated using a discretized version of the probability density function. The increase in computational speed, however, came at the cost of reduced accuracy.

To achieve accuracy without sacrificing efficiency, Evans and Dapino [33] developed a constitutive model for Galfenol by choosing orientations which minimize an energy function locally defined in the vicinity of each easy axis. The anisotropy energy  $G_A^k$  at a direction  $\mathbf{m}^k$  is formulated as

$$G_A^k = \frac{1}{2}K^k|\mathbf{m}^k - \mathbf{c}^k|^2,\tag{1}$$

where the constant  $K^k$  quantifies the anisotropy energy around the kth easy axis  $\mathbf{c}^k$ . The notation used to numerate these axes is presented in Fig. 1.

The anisotropy energy along each easy axis is zero, which applies to materials with cubic anisotropy such as unannealed Galfenol. However, it has been shown that stress annealing induces tetragonal anisotropy in Galfenol [35] where the four  $\langle 100 \rangle$  directions perpendicular to the annealing direction have a lower energy than the other two. To make the model capable of describing the effects of stress annealing, the anisotropy energy is modified as

$$G_A^k = \frac{1}{2}K|\mathbf{m}^k - \mathbf{c}^k|^2 + K_0^k,$$
 (2)

where K quantifies the anisotropy energy around all easy axes and  $K_0^k$  specifies the base anisotropy energy along the kth easy axis. Separating anisotropy energy parameters K and  $K_0^k$  makes it possible to derive the new generalized expressions for the partial derivatives  $\partial \mathbf{m}^k/\partial H_i$  and  $\partial \mathbf{m}^k/\partial T_{ij}$ , which are discussed in the procedure section. Further, the  $\mathbf{m}$ -dependent portion of the anisotropy energy remains unchanged, which means the minimization results remain unaffected. The total free energy around  $\mathbf{c}^k$  is formulated as the sum of the local anisotropy energy  $G_A^k$ , magnetomechanical coupling energy  $G_C^k$  and the Zeeman energy  $G_Z^k$  as

$$G^{k} = \underbrace{\frac{1}{2}K|\mathbf{m}^{k} - \mathbf{c}^{k}|^{2} + K_{0}^{k}}_{G_{A}^{k}} - \underbrace{\mathbf{S}_{m}^{k} \cdot \mathbf{T}}_{G_{C}^{k}} - \underbrace{\mu_{0}M_{s}\mathbf{m}^{k} \cdot \mathbf{H}}_{G_{Z}^{k}}, \tag{3}$$

where the magnetostriction tensor  $\mathbf{S}_m^k$  for a cubic material is defined as

$$\mathbf{S}_{m}^{k} = \left\{ \begin{array}{l} (3/2)\lambda_{100}(m_{1}^{k})^{2} \\ (3/2)\lambda_{100}(m_{2}^{k})^{2} \\ (3/2)\lambda_{100}(m_{3}^{k})^{2} \\ 3\lambda_{111}m_{1}^{k}m_{3}^{k} \\ 3\lambda_{111}m_{1}^{k}m_{3}^{k} \\ 3\lambda_{111}m_{1}^{k}m_{3}^{k} \end{array} \right\}, \tag{4}$$

and input stress and magnetic field vectors T and H are given as

$$\mathbf{T} = \begin{bmatrix} T_{11} & T_{22} & T_{33} & T_{12} & T_{23} & T_{13} \end{bmatrix}^{\mathbf{T}}, \tag{5}$$

$$\mathbf{H} = \begin{bmatrix} H_1 \\ H_2 \\ H_3 \end{bmatrix}. \tag{6}$$

The energy function can be represented in the matrix form as

$$G^{k} = \frac{1}{2}\mathbf{m}^{k} \cdot \mathbf{K}\mathbf{m}^{k} - \mathbf{m}^{k} \cdot \mathbf{B}^{k} + \frac{1}{2}K + K_{0}^{k}, \tag{7}$$

where the magnetic stiffness matrix **K** and force vector  $\mathbf{B}^k$  are

$$\mathbf{K} = \begin{bmatrix} K - 3\lambda_{100}T_{11} & -3\lambda_{111}T_{12} & -3\lambda_{111}T_{13} \\ -3\lambda_{111}T_{12} & K - 3\lambda_{100}T_{22} & -3\lambda_{111}T_{23} \\ -3\lambda_{111}T_{13} & -3\lambda_{111}T_{23} & K - 3\lambda_{100}T_{33} \end{bmatrix}, \tag{8}$$

$$\mathbf{B}^{k} = \left[ c_{1}^{k} K + \mu_{0} M_{s} H_{1} \ c_{2}^{k} K + \mu_{0} M_{s} H_{2} \ c_{3}^{k} K + \mu_{0} M_{s} H_{2} \right]^{\mathrm{T}}.(9)$$

Minimization of the energy function (7) based on the linearized unity norm constraint on the orientation vectors ( $\mathbf{m}^k \cdot \mathbf{m}^k = 1 \approx \mathbf{c}^k \cdot \mathbf{m}^k = 1$ ) yields an analytical expression for the orientation of the *k*th local minimum [33]

$$\mathbf{m}^{k} = (\mathbf{K})^{-1} \left[ \mathbf{B}^{k} + \frac{1 - \mathbf{c}^{k} \cdot (\mathbf{K})^{-1} \mathbf{B}^{k}}{\mathbf{c}^{k} \cdot (\mathbf{K})^{-1} \mathbf{c}^{k}} \mathbf{c}^{k} \right]. \tag{10}$$

The anhysteresis volume fractions are calculated through Boltzmann-type averaging [33] as

$$\xi_{an}^{k} = \frac{\exp\left(-G^{k}/\Omega\right)}{\sum_{s=\pm 1}^{\pm 3} \exp\left(-G^{s}/\Omega\right)},\tag{11}$$

where  $\Omega$  is an averaging factor. Then bulk magnetization, strain and magnetic induction can be obtained by summing the contribution of each domain weighted by the associated volume fraction [33] as

$$\mathbf{M} = M_s \sum_{k=+1}^{\pm 3} \boldsymbol{\xi}^k \mathbf{m}^k, \tag{12}$$

$$\mathbf{S} = \mathbf{s}\mathbf{T} + \sum_{k=1}^{\pm 3} \xi^k \mathbf{S}_m^k, \tag{13}$$

$$\mathbf{B} = \mu_0 \left( \mathbf{H} + \mathbf{M} \right) \tag{14}$$

where the compliance tensor is

$$\mathbf{s} = \begin{bmatrix} c_{11} & c_{12} & c_{13} & 0 & 0 & 0 \\ c_{12} & c_{11} & c_{23} & 0 & 0 & 0 \\ c_{13} & c_{23} & c_{11} & 0 & 0 & 0 \\ 0 & 0 & 0 & c_{44} & 0 & 0 \\ 0 & 0 & 0 & 0 & c_{55} & 0 \\ 0 & 0 & 0 & 0 & 0 & c_{66} \end{bmatrix}^{-1} . \tag{15}$$

Volume fraction of the kth orientation at ith time step is defined in incremental form [33] as

$$\xi^{k}(i+1) = \xi^{k}(i) + d\xi^{k}(i), \tag{16}$$

where the volume fraction increment  $d\xi^k$  consists of hysteresis component  $d\xi^k_{irr}$  which is due to irreversible domain wall motion

and anhysteresis component  $d\xi_{an}^k$  which is due to domain wall bowing [39]

$$d\xi^{k}(i) = (1 - c)d\xi^{k}_{irr}(i) + cd\xi^{k}_{an}(i), \tag{17}$$

where c is the weight of reversible rotation. Irreversible volume fraction increment is given [33] by

$$\begin{split} d\xi_{irr}^{k}(i) &= \frac{\zeta}{k_{p}} \left( \xi_{an}^{k}(i) - \xi^{k}(i) \right) \left[ \mu_{0} M_{s} \left( |dH_{1}(i)| + |dH_{2}(i)| \right. \\ &+ |dH_{3}(i)| \right) + \frac{3}{2} \lambda_{100} \left( |dT_{11}(i)| + |dT_{22}(i)| + |dT_{33}(i)| \right) \\ &+ 3\lambda_{111} \left( |dT_{12}(i)| + |dT_{13}(i)| + |dT_{23}(i)| \right) \right], \end{split}$$

$$(18)$$

where  $k_p$  quantifies pinning site density of the material,  $dH_i$  and  $dT_{ij}$  are the increment in field and stress components, respectively. The value of  $\zeta$  is one unless the resulting increment gives a negative susceptibility, in which case it is switched to zero. Specially, the anhysteresis response can be calculated by setting c=1. Since the anhysteresis volume fraction in kth direction is a function of inputs  $H_i$  and  $T_{ij}$ , chain rule gives

$$d\xi_{an}^{k} = \frac{\partial \xi_{an}^{k}}{\partial H_{i}} dH_{i} + \frac{\partial \xi_{an}^{k}}{\partial T_{ij}} dT_{ij}, \tag{19}$$

where the derivatives of  $\xi_{an}^k$  with respect to  $H_i$  and  $T_{ij}$  are

$$\frac{\partial \xi_{an}^{k}}{\partial H_{i}} = \frac{\xi_{an}^{k}}{\Omega} \left[ \sum_{n=\pm 1}^{\pm 3} \xi_{an}^{n} \left( \frac{\partial G^{n}}{\partial H_{i}} \right) - \left( \frac{\partial G^{k}}{\partial H_{i}} \right) \right], \quad (20)$$

$$\frac{\partial \xi_{an}^{k}}{\partial T_{ij}} = \frac{\xi_{an}^{k}}{\Omega} \left[ \sum_{n=\pm 1}^{\pm 3} \xi_{an}^{n} \left( \frac{\partial G^{n}}{\partial T_{ij}} \right) - \left( \frac{\partial G^{k}}{\partial T_{ij}} \right) \right]. \tag{21}$$

The derivatives of  $G^k$  with respect to  $H_i$  and  $T_{i,i}$  are

$$\frac{\partial G^k}{\partial H_i} = \mathbf{m}^k \cdot \mathbf{K} \left( \frac{\partial \mathbf{m}^k}{\partial H_i} \right) - \frac{\partial \mathbf{m}^k}{\partial H_i} \cdot \mathbf{B}^k - \mathbf{m}^k \cdot \left( \frac{\partial \mathbf{B}^k}{\partial H_i} \right), \quad (22)$$

$$\frac{\partial G^k}{\partial T_{ij}} = \mathbf{m}^k \cdot \mathbf{K} \left( \frac{\partial \mathbf{m}^k}{\partial T_{ij}} \right) + \frac{1}{2} \mathbf{m}^k \cdot \left( \frac{\partial \mathbf{K}}{\partial T_{ij}} \right) \mathbf{m}^k - \frac{\partial \mathbf{m}^k}{\partial T_{ij}} \cdot \mathbf{B}^k (23)$$

In this paper, to reduce computational time, new generalized expressions for the partial derivatives  $\partial \mathbf{m}^k/\partial H_i$  and  $\partial \mathbf{m}^k/\partial T_{ij}$  are presented,

$$\frac{\partial \mathbf{m}^k}{\partial H_i} = \mu_0 M_s \mathbf{X}_i^k,\tag{24}$$

$$\frac{\partial \mathbf{m}^k}{\partial T_{ij}} = \begin{cases} 3\lambda_{100}(\mathbf{X}_i^k \phi_i) \mathbf{m}^k & \text{if } i = j\\ 3\lambda_{111}(\mathbf{X}_i^k \phi_j + \mathbf{X}_j^k \phi_i) \mathbf{m}^k & \text{if } i \neq j, \end{cases}$$
(25)

where

$$\phi_i = \left[ \delta(i,1) \ \delta(i,2) \ \delta(i,3) \right], \tag{26}$$

$$\mathbf{X}_{i}^{k} = \begin{cases} \begin{bmatrix} 0 & 0 & 0 \end{bmatrix}^{\mathrm{T}} & \text{if } i = |k| \\ \phi_{i}^{\mathrm{T}} R_{n(i,k)} + 3\lambda_{111} \phi_{n(i,k)}^{\mathrm{T}} T_{p(k)q(k)} \\ R_{n(k)} R_{q(k)} - (3\lambda_{111} T_{n(k)q(k)})^{2} & \text{if } i \neq |k| \,, \end{cases}$$
(27)

$$R_i = K - 3T_i\lambda_{100},\tag{28}$$

 $\delta$  is the Kronecker delta function, and indices p, q, and n represent perpendicularity such that

$$D = \{1, 2, 3\},\tag{29}$$

$$\{p(k), q(k)\} = D/\{k\},$$
 (30)

$$n(i,k) = D/\{i,k\}.$$
 (31)

#### PARAMETER OPTIMIZATION PROCEDURE

The model parameters are the seven anisotropy constants K,  $K_0^1$ ,  $K_0^{-1}$ ,  $K_0^2$ ,  $K_0^{-2}$ ,  $K_0^3$ , and  $K_0^{-3}$ , magnetostriction constants  $\lambda_{100}$  and  $\lambda_{111}$ , smoothing factor  $\Omega$ , saturation induction  $\mu_0 M_s$ , pinning site density parameter  $k_p$ , the weight of reversible rotation c, and moduli coefficients  $c_{11}$ ,  $c_{12}$ ,  $c_{13}$ ,  $c_{23}$ ,  $c_{44}$ ,  $c_{55}$ , and  $c_{66}$ . Stress annealing induces anisotropy energy only in the two directions parallel to the axis of the rod, which are chosen to be k = 1 and k = -1. The remaining four directions perpendicular to the annealing orientation are symmetrical about the axis of the rod, and thus are equivalent in energy. For this reason, the base anisotropy constants are split into two groups:  $K_{0_{\parallel}}$  and  $K_{0_{\perp}}$ . The parameter  $K_{0\parallel}$  is the anisotropy energy for the two orientations parallel to the axis of the rod, while  $K_{0+}$  is the anisotropy constant for the four orientations perpendicular to the axis of the rod, k = 2, k = -2, k = 3, and k = -3. Since we are interested only in the relative anisotropy energies,  $K_{0+}$  is chosen to be zero and  $K_{0+}$ will be called  $K_0$  for simplicity. Thus, the total number of unknown parameters is reduced to fifteen. As shown in Tab. 1, fifteen model parameters are divided into three groups: anhysteresis parameters, hysteresis parameters, and higher-dimensional parameters that have no effect on the 1D stress and field applications. The anhysteresis parameters describe the overall shape

**TABLE 1**. GROUPS OF PARAMETERS INVOLVED IN THE DEA MODEL.

Anhysteresis	$\mu_0 M_s, \lambda_{100}, c_{11},$
parameters	$K, K_0, \Omega$
Hysteresis	k a
parameters	$k_p, c$
Higher-dimensional	$\lambda_{111}, c_{12}, c_{13}, c_{23},$
parameters	$c_{44}, c_{55}, c_{66}$

of the curves, while the hysteresis parameters only control the hysteresis size.

The aim of parameter optimization is to minimize an error function which describes the discrepancy between the experimental data and the DEA modeling results. The error function for the *i*th curve in a data set is given as

$$error_i = \frac{1}{range(\mathbf{X}_i)} \sqrt{\frac{\sum_{j=1}^{N_i} (Y_{ij} - X_{ij})^2}{N_i}},$$
 (32)

where  $Y_{ij}$  and  $X_{ij}$  are the *j*th component of the *i*th model and data vectors, respectively, each containing  $N_i$  points, and  $range(\mathbf{X}_i)$  is the range of the *i*th data vector.

The parameter optimization process introduced by this work consists of four steps. First, anhysteresis curves are obtained from hysteresis measurements through an averaging procedure. Second, initial values of anhysteresis parameters are estimated from anhysteresis curves. Third, a least squares optimization routine is used to minimize the error function defined in (32) and obtain the anhysteresis parameters, since the overall shape of the curves depends mostly on the anhysteresis parameters. Finally, a second optimization is run on the hysteresis data to determine hysteresis parameters. A representative flowchart is presented in Fig. 2.

## Extracting the anhysteresis curves from measurements

The anhysteresis curves are obtained by computing an average value from the upper and lower branches of the hysteresis loops. As pointed out by Benbouzid et al. [28], this procedure yields an approximate anhysteresis value and may not coincide with experimental anhysteresis curves obtained by superimposing a decaying AC component of the input variable, field or stress, about a mean value. The anhysteresis curves are obtained by sweeping the varying input over the entire applied range at discrete steps and finding an average value within each step. For

example, the anhysteresis strain at a field  $H_0$  under varying magnetic field, and anhysteresis magnetic induction at a stress  $T_0$  under varying stress are computed as

$$B_{an}(T_0) = AVG(B(T): T_0 - \delta_T < T < T_0 + \delta_T),$$
 (33)

$$S_{an}(H_0) = AVG(S(H): H_0 - \delta_H < H < H_0 + \delta_H),$$
 (34)

where  $\delta_H$  and  $\delta_T$  are field and stress increments. In general, a large value introduces error due to averaging over a wider range of input while a very small  $\delta_H$  or  $\delta_T$  might result in non-existence of a data point in that range. In this study,

$$\delta_H = 20 \text{ A/m}, \text{ and } \delta_T = 30 \text{ kPa}.$$
 (35)

Since the anhysteresis model is in incremental form, anhysteresis averaging is a good method to lower the sampling frequency from the rate which it was collected. This is useful because fewer number of data points means the model would be executed fewer times, consuming less computation time.

#### Estimating anhysteresis parameters

The efficiency of the optimization algorithm can be greatly enhanced by estimating parameters from anhysteresis curves and fixing parameters that are not expected to change. Values of  $\mu_0 M_s$ ,  $\lambda_{100}$ ,  $c_{11}$ , K, and  $K_0$  are estimated and parameters  $\mu_0 M_s$ ,  $\lambda_{100}$ , and  $c_{11}$  are fixed after estimation. The parameters  $\mu_0 M_s$ ,  $\lambda_{100}$ , and  $c_{11}$  can be directly obtained from the saturated induction, the saturated magnetostriction, and the slope of stress-strain curves at saturation regions, respectively, as shown in Fig. 3.

The anisotropy constant K is estimated from the slope  $\mu(T)$  of the extracted anhysteresis induction versus field curve for a given stress T at zero field. The slope is computed numerically at a low magnetic field and substituted into the stress-dependent susceptibility expression derived by Evans and Dapino [40], giving

$$K = 3\lambda_{100}T + \frac{(\mu_0 M_s)^2}{\mu(T) - \mu_0}. (36)$$

The anisotropy constant  $K_0$  can be estimated from the location of the burst region, which depends on the Gibbs energy

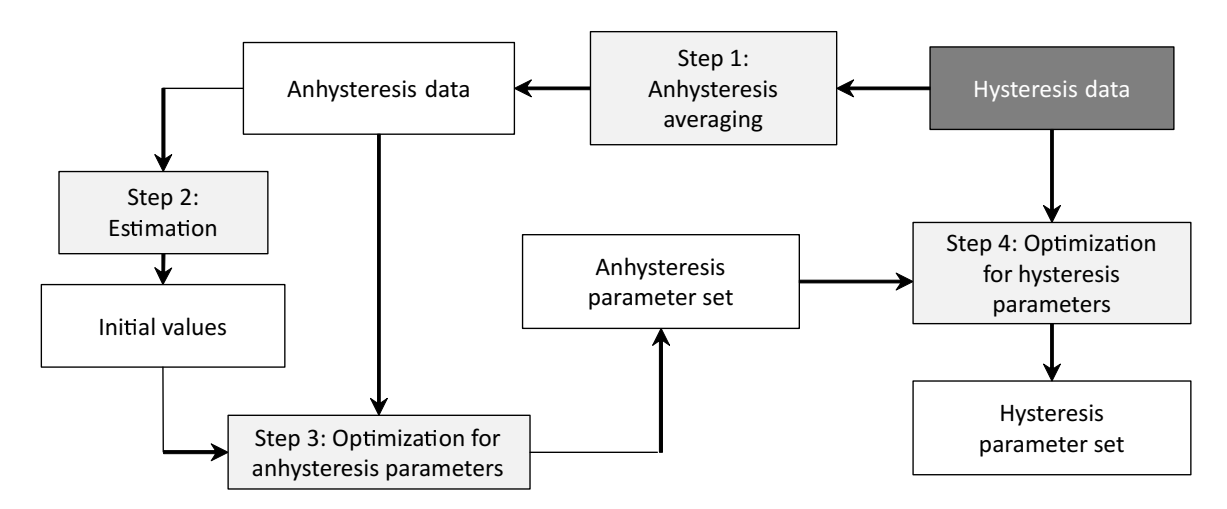
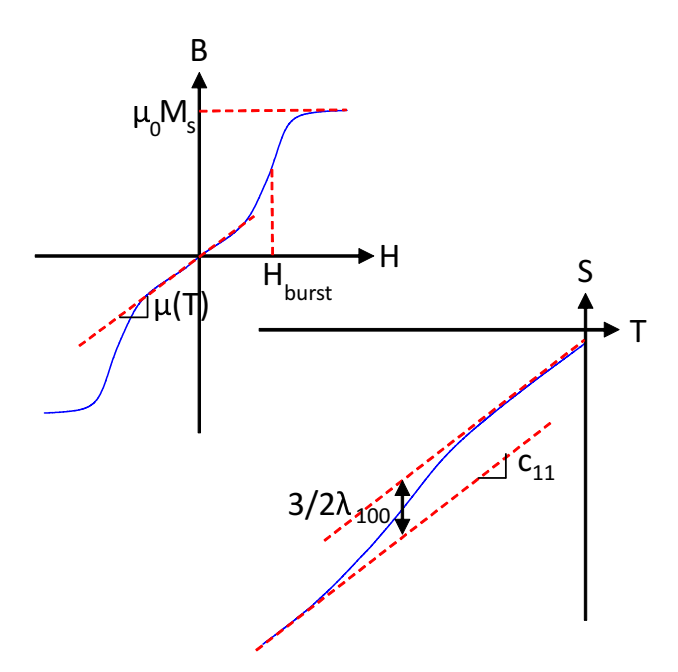


FIGURE 2. SCHEMATIC REPRESENTATION FOR THE PARAMETER OPTIMIZATION ALGORITHM INTRODUCED IN THIS WORK.



FEATURES IN INDUCTION VERSUS FIELD AND FIGURE 3. STRAIN VERSUS STRESS PLOTS THAT ARE USED FOR ESTI-MATING MODEL PARAMETERS.

along the directions perpendicular and parallel to the direction of application of field. These energies are given [40] by

$$E_{\perp} = \frac{(\mu_0 M_s H)^2}{6\lambda_{100} T - 2K},$$

$$E_{\parallel} = -\frac{3}{2}\lambda_{100} T - \mu_0 M_s H + K_0.$$
(37)

$$E_{\parallel} = -\frac{3}{2}\lambda_{100}T - \mu_0 M_s H + K_0. \tag{38}$$

The burst phenomenon occurs when the energies of two orientations become roughly equal and domains start flipping from one orientation to the other. In this study, the burst field  $H_{burst}$  is obtained by selecting the magnetic field in which the gradient of the induction versus field curve is maximum. Equating (37) and (38) gives

$$K_0 = \frac{3}{2}\lambda_{100}T + \frac{(\mu_0 M_s H_{burst})^2}{6\lambda_{100}T - 2K} + \mu_0 M_s H_{burst}.$$
 (39)

To improve optimization efficiency, this study fixes parameters  $\mu_0 M_s$ ,  $\lambda_{100}$ , and  $c_{11}$  which can be accurately estimated from obvious features of the plots. However, the estimation of parameters K and  $K_0$  is less accurate, since estimating the slope of induction versus field curve and the location of burst region introduce uncertainty. Hence, K and  $K_0$  need to be optimized. The validation of this practice is studied in the results section.

#### Optimization for anhysteresis parameters

The least squares optimization is conducted using the MAT-LAB function fmincon. This function needs initial guesses, bounds for each parameter, and a scalar error definition which it minimizes. The parameters K and  $K_0$  are given  $\pm 60\%$  bounds relative to their estimated values. The parameter  $\Omega$  is given an initial guess of 1100 J/m<sup>3</sup> and a bound of  $\pm 80\%$  relative to the initial guess. The error definition is constructed as follows

$$E = \frac{1}{y} \sum_{i=1}^{y} error_i \tag{40}$$

**TABLE 2**. OPTIMIZED DEA MODEL PARAMETERS, CORRESPONDING MODELING ERROR, AND AVERAGE CPU TIME ELAPSED DURING OPTIMIZATION FOR AN UNANNEALED TEXTURED POLYCRYSTALLINE  $fe_{81.6}Ga_{18.4}$  SAMPLE GROWN WITH FSZM.

Parameters									Average
$\mu_0 M_s$	$\mu_0 M_s$ 3/2 $\lambda_{100}$ $c_{11}$ $K$ $K_0$ $\Omega$ $k_p$ $C$								
(T)	$(\times 10^{-6})$	(GPa)	$(kJ/m^3)$	$(kJ/m^3)$	$(kJ/m^3)$	$(kJ/m^3)$	(-)	(%)	time (s)
1.575	233.503	70.740	18.074	0.222	0.933	0.311	0.855	1.45	71.96

where y is the total number of curves. A random parameter search, as described by Deng et al. [41], is utilized where N initial guesses are randomly chosen within the bounds, and the optimized set that returns the least modeling error is assumed to be the global minimum.

#### Optimization for hysteresis parameters

Optimized anhysteresis parameters are used as initial guesses in the hysteresis optimization step with a narrower bound of  $\pm 20\%$ . The hysteresis parameters  $k_p$  and c are given initial values of 230 J/m³ and 0.5, and given bounds of  $\pm 80\%$  and  $\pm 100\%$ , respectively. The random parameter search and error definition (40) are employed in the hysteresis optimization routine.

#### **RESULTS**

This section is divided into two parts in order to thoroughly evaluate the performance of the proposed optimization algorithm. First, the performance of all optimization techniques presented in the procedure section are tested using measurements on an unannealed textured polycrystalline Fe<sub>81.6</sub>Ga<sub>18.4</sub> sample. Second, the optimization algorithm is validated using measurements from multiple Galfenol specimens with various compositions and heat treatments. All the computations are done with an Intel Xeon 3.50 GHz CPU and 32.0 GB RAM desktop computer.

#### Evaluation of the parameter optimization algorithm

Following the procedure in Fig. 2, the resulting DEA model parameters of an unannealed textured polycrystalline  $Fe_{81.6}Ga_{18.4}$  sample are presented in Tab. 2, and the associated modeling results are plotted on top of measurements in Fig. 4.

The convergence of the algorithm is tested by running the algorithm with 50 random initial guesses and calculating the range of corresponding optimized parameters. Figure 6 shows that the deviation of optimized material properties obtained from different initial guesses is negligible and thus the algorithm is assumed to converge to a global minimum.

The effectiveness of the generalized partial derivative expressions and the optimization steps are studied in detail.

### Generalized expressions for partial derivatives

The efficiency of the DEA model, which is quantified by the computational time, is compared for traditional partial derivative expressions [23] and the generalized expressions proposed in the DEA model section as shown in Fig. 5. This study shows that the generalized expressions improve the efficiency by 61% on average.

**Estimating anhysteresis parameters** The benefit of estimating parameters from the anhysteresis data is studied first. To run the algorithm without the estimation step, initial guesses are cited from [42], in which case broader bounds are needed to ensure a global minimum for the optimization algorithm. The results of this study, which are presented in Tab. 3, show that not estimating  $\mu_0 M_s$ ,  $\lambda_{100}$ ,  $c_{11}$ , K, and  $K_0$  decreases accuracy and efficiency by 3.5% and 22%, respectively. This poorer performance is due to the fact that the algorithm needs to search for a global minimum over a wider range of parameters.

Second, the benefit of fixing parameters  $\mu_0 M_s$ ,  $\lambda_{100}$ , and  $c_{11}$  is evaluated by comparing the efficiency and accuracy when the complete set of parameters are optimized. As presented in Tab. 4, the accuracy reduces by 0.06% when  $\mu_0 M_s$ ,  $\lambda_{100}$ , and  $c_{11}$  are fixed, while the efficiency is improved by 41%.

Hence, fixing these parameters contributes to efficiency significantly without sacrificing accuracy.

**Two-step optimization algorithm** An alternative algorithm is constructed where optimization routine is performed directly on hysteresis data in order to test the two-step optimization. The results of one-step optimization, which are presented in Tab. 5, show that the two-step optimization algorithm improves the efficiency and accuracy by 28% and 0.26%, respectively.

#### Application to different specimens

The proposed parameter optimization algorithm is applied to specimens with different compositions and heat treatments. Due to the lack of hysteresis data in the literature, only anhysteresis parameters are presented in Tab. 6. DEA model parameters  $\mu_0 M_s$ ,  $\lambda_{100}$ , K, and  $K_0$  are plotted against gallium content in Fig. 7.

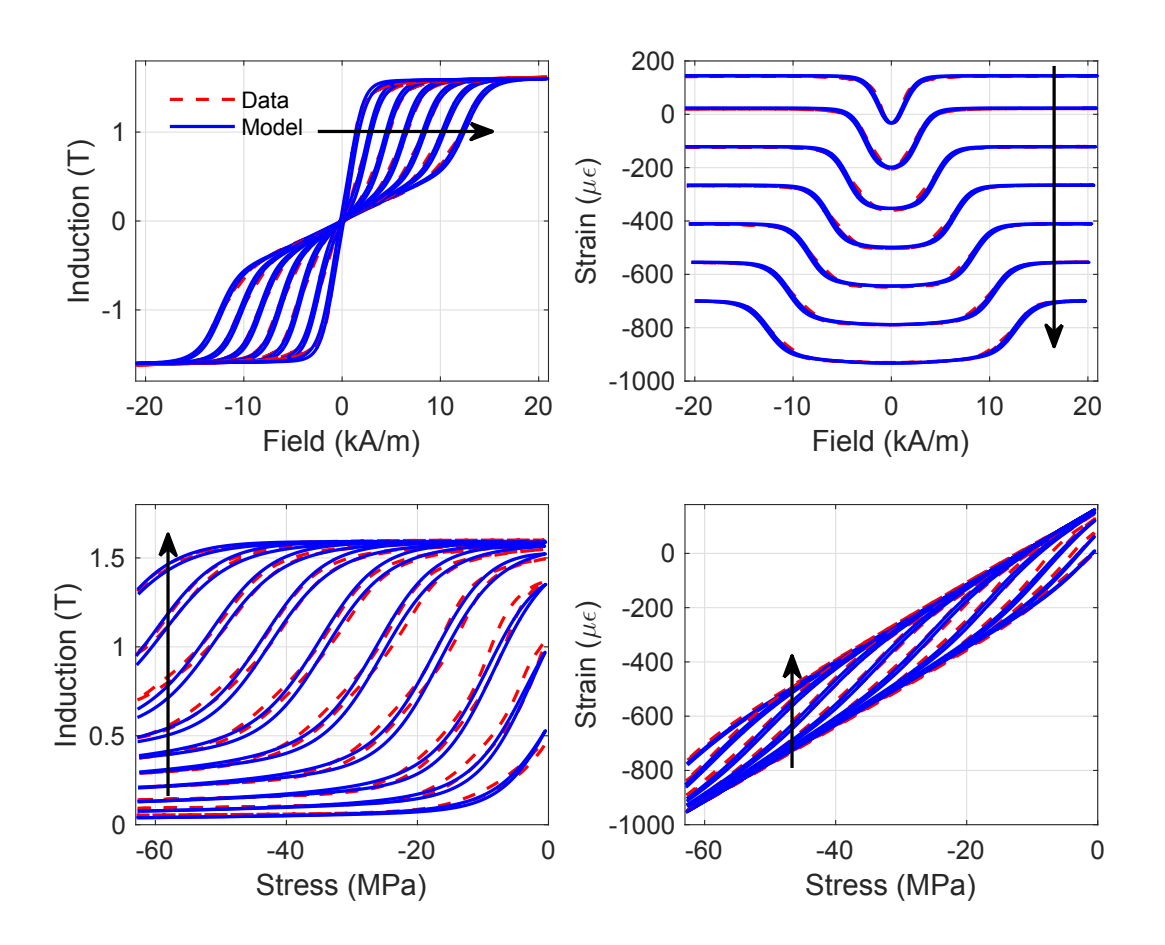


**FIGURE 4**. COMPARISON OF MEASUREMENTS AND HYSTERESIS CURVES FROM THE MODEL AT CONSTANT COMPRESSIVE STRESSES OF 1.64, 10.23, 20.44, 30.65, 40.88, 51.10, AND 61.31 (MPa) AND CONSTANT FIELD VALUES OF 0.73, 1.42, 2.41, 3.88, 5.50, 7.17, 8.84, 10.51, 12.19 AND 13.76 (kA/m). ARROWS INDICATE INCREASING COMPRESSIVE STRESS OR BIAS FIELD.

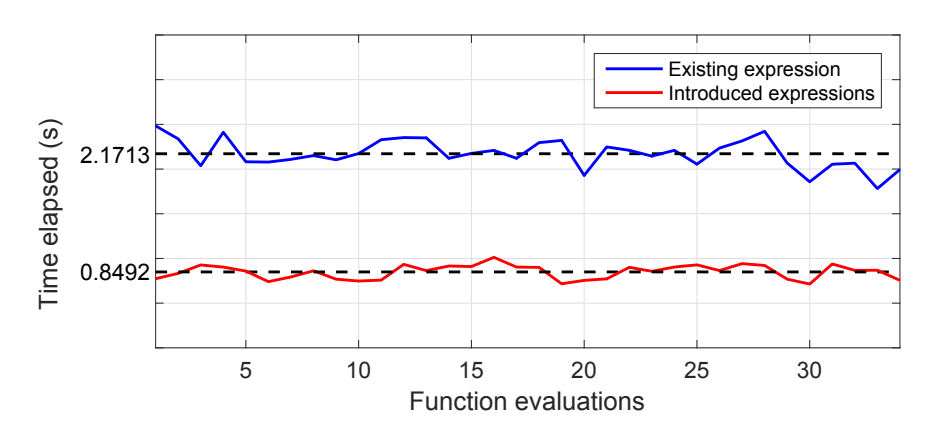


**FIGURE 5**. COMPARISON OF CPU TIME ELAPSED FOR TWO DEA MODELS, ONE OF WHICH IS USING PREVIOUS PARTIAL DERIVATIVE EXPRESSIONS AND THE OTHER USING GENERALIZED EXPRESSIONS INTRODUCED IN THIS WORK. THE MODEL IS RUN ON 1380 DATA POINTS.

**TABLE 3.** OPTIMIZED DEA MODEL PARAMETERS, CORRESPONDING MODELING ERROR AND AVERAGE CPU TIME ELAPSED WHEN INITIAL GUESS ESTIMATIONS ARE NOT USED.

Parameters									Average
$\mu_0 M_s$	$M_s$ 3/2 $\lambda_{100}$ $c_{11}$ $K$ $K_0$ $\Omega$ $k_p$ $C$							Error	CPU
(T)	$(\times 10^{-6})$	(GPa)	$(kJ/m^3)$	$(kJ/m^3)$	$(kJ/m^3)$	$(kJ/m^3)$	(-)	(%)	time (s)
1.550	255.000	70.000	18.094	0.222	0.933	0.311	0.855	4.96	87.71

**TABLE 4.** OPTIMIZED DEA MODEL PARAMETERS, CORRESPONDING MODELING ERROR, AND AVERAGE CPU TIME ELAPSED WHEN FULL SET OF PARAMETERS ARE OPTIMIZED.

Parameters									Average
$\mu_0 M_s$	$\mu_0 M_s$ 3/2 $\lambda_{100}$ $c_{11}$ $K$ $K_0$ $\Omega$ $k_p$ $C$								
(T)	$(\times 10^{-6})$	(GPa)	$\left(kJ/m^3\right)$	$\left(kJ/m^3\right)$	$(kJ/m^3)$	$(kJ/m^3)$	(-)	(%)	time (s)
1.577	228.232	70.676	16.505	0.278	0.959	0.221	0.800	1.39	122.65

**TABLE 5.** OPTIMIZED DEA MODEL PARAMETERS, CORRESPONDING MODELING ERROR, AND AVERAGE CPU TIME ELAPSED WHEN ONLY ONE OPTIMIZATION PROCEDURE IS APPLIED DIRECTLY ON HYSTERESIS DATA.

Parameters									Average
$\mu_0 M_s$	$\mu_0 M_s$ 3/2 $\lambda_{100}$ $c_{11}$ $K$ $K_0$ $\Omega$ $k_p$ $C$								
(T)	$(\times 10^{-6})$	(GPa)	$(kJ/m^3)$	$(kJ/m^3)$	$(kJ/m^3)$	$(kJ/m^3)$	(-)	(%)	time (s)
1.575	233.503	70.740	18.726	0.278	0.940	0.311	0.858	1.71	100.15

Some observations can be made from Fig. 7:

- 1. Saturation induction  $\mu_0 M_s$  decreases with increasing Ga content as presented in [46]. This is possibly attributed to diamagnetic gallium atoms that weaken ferromagnetic properties of iron.
- 2. For single crystal specimens, saturation magnetostriction  $\lambda_{100}$  peaks around 19% Ga and 27% Ga; this phenomenon is attributed to the magnetoelastic energy that increases rapidly for small concentrations up to 19% Ga and a near-linear softening of the shear elastic constant extending to 27% Ga [47].
- 3. Quenched single crystal material has a significantly higher base anisotropy energy *K* than the furnace cooled specimen of the same Ga content. This is possibly because quenching is an orientation-independent process and induces higher internal energy in all directions.
- 4. Annealed polycrystalline material has a significantly higher anisotropy energy  $K_0$  in the two orientations parallel to the axis of the rod, which are the stress annealing directions, since annealing induces a uniaxial anisotropy in [100] and  $\lceil \bar{1}00 \rceil$  orientations.
- 5. Single crystal and polycrystalline specimens with the same

Ga content have similar base anisotropy energy *K*.

In order to verify the trends in parameters and relate them to the performance of the proposed optimization algorithm, the effect of each parameter on the modeling error is investigated. To that end, a sensitivity function is defined as

$$\delta_i = \frac{\partial E}{\partial p_i} \tag{41}$$

where E is the scalar error defined in (40), and  $p_i$  is the ith model parameter. These partial derivatives are calculated numerically, and the sensitivity of the modeling error for  $\mu_0 M_s$ ,  $\lambda_{100}$ , and  $c_{11}$  is found to be much higher than K,  $K_0$ ,  $\Omega$ ,  $k_p$ , and c. This result coincides with a previous study [41] where the uncertainty in K,  $K_0$ ,  $\Omega$ ,  $k_p$ , and c has proven to be more significant than  $\mu_0 M_s$ ,  $\lambda_{100}$ , and  $c_{11}$  at a given measurement error. Due to the high uncertainty in optimized K and  $K_0$ , no clear trends can be seen in Fig. 7. However, any arbitrary values selected from the range provided in Fig. 7 can be used as initial guesses to obtain high accuracy in model results.

**TABLE 6.** OPTIMIZED ANHYSTERESIS PARAMETERS OF DEA MODEL AND CORRESPONDING MODELING ERROR FOR SEVERAL SPECIMENS.(C: CRYSTAL STRUCTURE, S: SINGLE CRYSTAL, P: POLYCRYSTALLINE; HT: HEAT TREATMENT, F: FURNACE COOLED, U: UNANNEALED, A: ANNEALED, Q: QUENCHED; \* ONLY B VERSUS H CURVES ARE USED FOR OPTIMIZATION, \*\* MODULUS DATA IS NOT AVAILABLE FOR MOST CASES)

Ga			$\mu_0 M_s$	$3/2\lambda_{100}$	c <sub>11</sub> **	K	<i>K</i> <sub>0</sub>	Ω	Error	
(at%)	С	НТ	(T)	$(\times 10^{-6})$	(GPa)	$(kJ/m^3)$	$(kJ/m^3)$	$(kJ/m^3)$	(%)	Ref.
15	S	F	1.875	244.520	-	38.247	-18.928	7.187	1.56*	[45]
16	S	F	1.834	237.939	-	3.956	-1.942	1.015	3.75	[46]
17	S	F	1.773	267.118	-	$3.667 \times 10^{-8}$	-14.165	5.097	2.02*	[47]
18.4	P	U	1.575	233.503	70.740	18.074	0.222	0.933	1.45	[41]
18.4	P	A	1.565	250.270	-	56.277	11.918	2.174	1.42	[48]
18.5	P	U	1.573	270.418	56.153	37.597	0.459	0.933	4.47	[33]
19	S	F	1.625	301.078	-	50.049	-2.274	1.556	1.59	[32]
19	S	Q	1.530	274.413	-	489.067	-18.593	5.271	1.58*	[49]
20.9	S	F	1.226	215.677	-	8.390	2.302	0.937	1.96	[33]
20.9	P	U	1.465	184.683	-	8.929	0.843	0.891	5.29	[36]
24.7	S	F	1.339	278.022	-	0.744	0.949	2.104	2.94	[32]
29	S	F	1.098	257.893	-	4.193	0.199	1.950	3.55	[32]

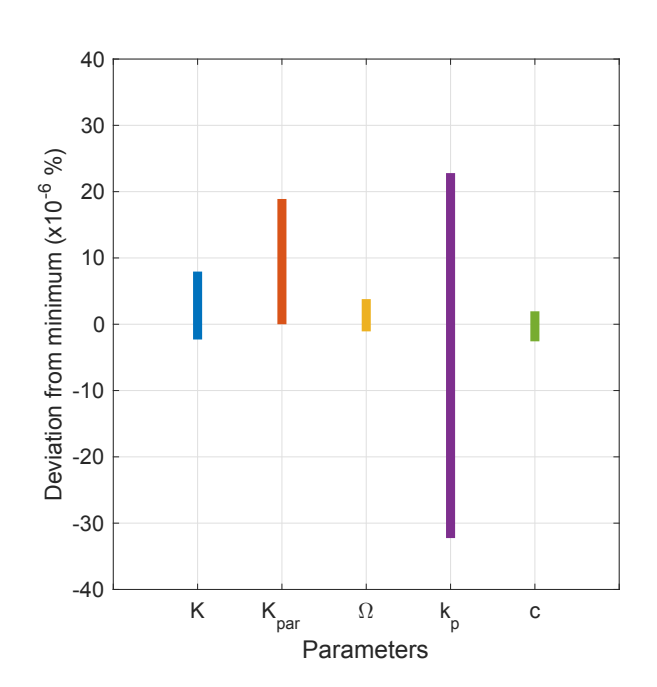


**FIGURE 6.** DEVIATION OF OPTIMIZED PARAMETERS FOR 50 SETS OF RANDOM INITIAL GUESSES.

#### CONCLUSION

Generalized partial derivative expressions, that are able to improve the efficiency by 61% on average relative to existing partial derivative expressions, are first developed for the DEA model. A universal and efficient optimization algorithm to find the DEA model parameters for Galfenol is introduced which consists of four steps, extracting the anhysteresis curves from measurements, estimating anhysteresis parameters, optimization for anhysteresis parameters, and optimization for hysteresis parameters. The performance of each step is evaluated in terms of efficiency and accuracy. Estimating and fixing parameters  $\mu_0 M_s$ ,  $\lambda_{100}$ , and  $c_{11}$  improves the efficiency by 41%, while preserving accuracy, relative to the case where these parameters are not estimated. This study shows another efficiency improvement of 28% by dividing the optimization into two-steps, anhysteresis and hysteresis. These results provide guidelines for future optimization studies. For instance, depending on the requirements of accuracy and efficiency, a system designer has the freedom to turn on or off certain steps of the algorithm. The optimization algorithm is then applied to multiple Galfenol samples with different Ga contents and heat treatments. Trends in DEA model parameters are presented which allow researchers to preliminarily select model parameters for other Galfenol samples whose characterization data is not available. For parameters K and  $K_0$ ,

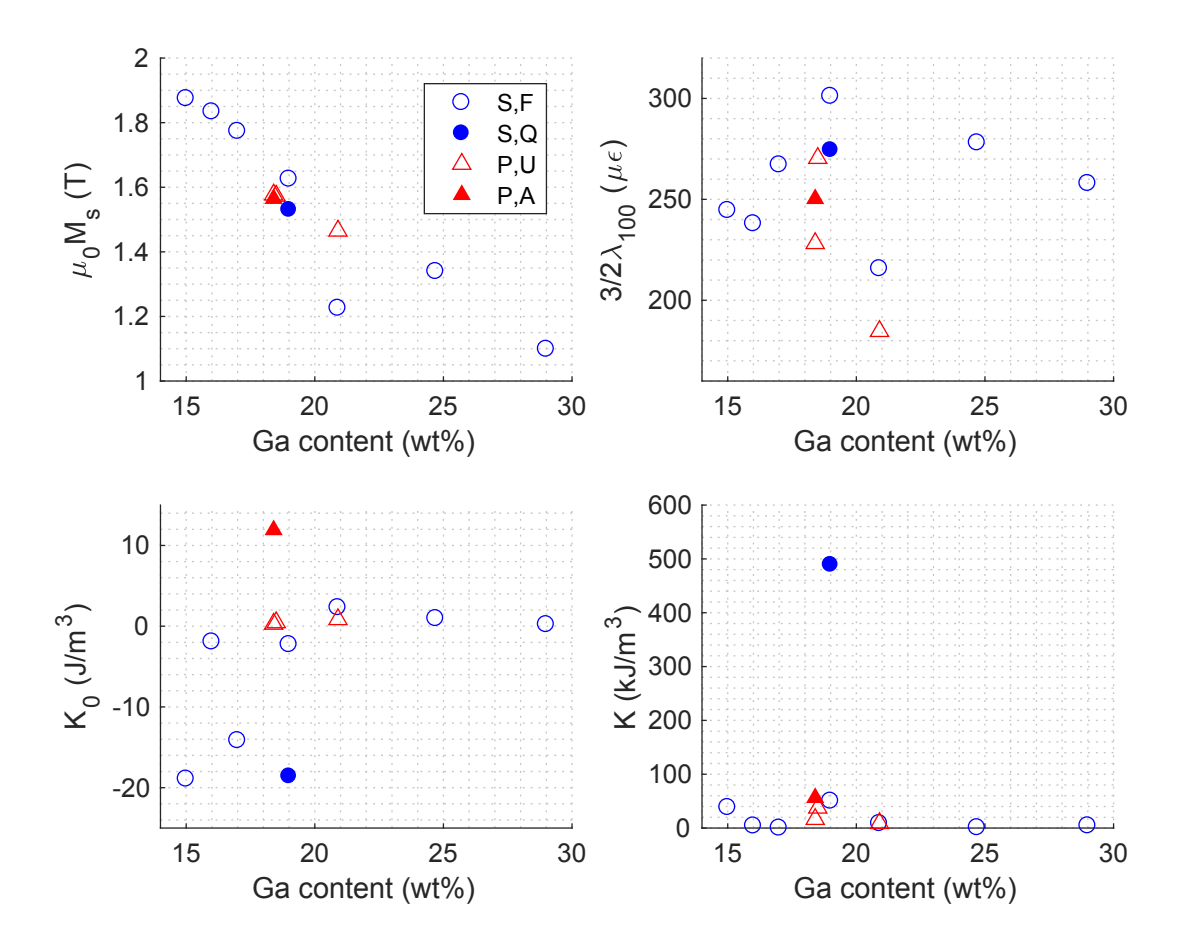


**FIGURE 7.** DEA PARAMETERS VERSUS GALLIUM CONTENT FOR DIFFERENT MATERIAL COMPOSITIONS AND HEAT TREATMENTS.

however, the trend is not clear due to the large uncertainty. Still, selecting K,  $K_0$ ,  $k_p$ , and c within the range provided by this paper can provide high accuracy. This work can be complemented by a future work that uses fully 3D measurements to evaluate higher-dimensional parameters.

#### **ACKNOWLEDGMENT**

We wish to acknowledge the financial support from the member organizations of the Smart Vehicle Concepts Center, a National Science Foundation Industry/University Cooperative Research Center established under NSF Grant IIP-1238286.

#### **REFERENCES**

[1] Ueno, T. and Yamada, S., 2011. *IEEE Transactions on Magnetics* 47 2407–9

- [2] Yoo, J. and Flatau, A. B., 2012. *Journal of Intelligent Material Systems and Structures* 23(6) 647–54.
- [3] Deng, Z. and Dapino, M. J., 2015. Smart Materials and Structures 24 125019.
- [4] Rezaeealam, B., Ueno, T., and Yamada, S., 2012. *IEEE Transactions on Magnetics* 48 3977–80.
- [5] Mudivarthi, C., Datta, S., Atulasimha, J., and Flatau, A., 2008. Smart Materials and Structures 17 035005.
- [6] Hale, K. and Flatau, A., 2006. Proc. SPIE 6173 61730Y.
- [7] McGary, P. D., Tan, L., Zou, J., Stadler, B. J. H., Downey, P. R., and Flatau, A. B., 2006. *Journal of Applied Physics* 99 08B310.
- [8] Yoo, J., Marschner, U., and Flatau, A. B., 2005. *Proc. SPIE* 5764 111–9.
- [9] Datta, S., Atulasimha, J., and Flatau, A. B., 2007. *Journal of Applied Physics* 101 09C521.
- [10] Ueno, T., Summers, E., and Higuchi, T., 2007. Sensors and Actuators A 137 134–40.

- [11] Ueno, T., Summers, E., Wun-Fogle, M., and Higuchi, T., 2008. *Sensors and Actuators A* 148 280–84.
- [12] Shu, L., Dapino, M. J., Evans, P. G., Chen, D., and Lu, Q., 2011. *Journal of Intelligent Material Systems and Structures* 22 781–93.
- [13] Ueno, T. and Higuchi, T., 2008. *IEEE Transactions on Magnetics* 44 4078–80.
- [14] Ueno, T., Saito, C., Imaizumi, N., and Higuchi, T., 2009. *Sensors and Actuators A* 154 92–6.
- [15] Deng, Z., Asnani, V. M., and Dapino, M. J., 2015. *Proc. SPIE* 9433 94330C.
- [16] Scheidler, J. J. and Dapino, M. J., 2013. Smart Materials and Structures 22 085015.
- [17] Yoo, J., Murray, A., and Flatau, A. B., 2014. Proc SPIE 9057 90573I.
- [18] Deng, Z. and Dapino, M. J., 2015. *Proc SPIE* 9433 94330B.
- [19] Shu, L., Wu, L., Wu, G., and Wu, Z., 2016. *IEEE Transactions on Magnetics* 52 8001607.
- [20] Zhou, H. and Zhou, Y., 2007. Smart Materials and Structures 16 198–206.
- [21] Rezaeealam, B., 2012. The International Journal for Computation and Mathematics in Electrical and Electronic Engineering 31 1757-1773.
- [22] Pérez-Aparicio, J. and Sosa, H., 2004. *Smart Materials and Structures* 13 493–502.
- [23] Chakrabarti, S. and Dapino, M. J., 2011. Smart Materials and Structures 20 105034.
- [24] Scheidler, J. J., Asnani, V. M., and Dapino, M. J., 2016. Smart Materials and Structures 25 035007.
- [25] Braghin, F., Cinquemani, S., and Resta, F., 2011. Sensors and Actuators A 165 342-50.
- [26] Chakrabarti, S. and Dapino, M. J., 2010. *Smart Materials and Structures* 19 055009.
- [27] Wang, L. and Yuan, F. G., 2008. Smart Materials and Structures 17 045009.
- [28] Benbouzid, M., Reyne, G., Meunier, G., Kvarnsjo, L., and Engdahl, G., 1995. *IEEE Transactions on Magnetics* 31 1821–1824 ISSN 0018-9464.
- [29] Kannan, K. and Dasgupta, A., 1997. *Smart Materials and Structures* 6 341–350.
- [30] Kim, J. and Jung, E., 2005. *Smart Materials and Structures* 14 1273–1280.
- [31] Armstrong, W., 1997. *Journal of Applied Physics* 81 23217–2326.
- [32] Atulasimha, J., Akhras, G., and Flatau, A. B., 2008. *Journal of Applied Physics* 103 07B336.
- [33] Evans, P. G. and Dapino, M. J., 2010. *Journal of Applied Physics* 107 063906.
- [34] Clark, A. E., Hathaway, K. B., Wun-Fogle, M., Restorff, J. B., Lograsso, T. A., Keppens, V. M., Petculescu, G., and Taylor, R. A., 2003. *Journal of Applied Physics* 93 8621– 8624.

- [35] Restorff, J., Wun-Fogle, M., Clark, A., and Hathaway, K., 2006. *IEEE Transactions on Magnetics* 42 3087–3089.
- [36] Mahadevan, A., Evans, P., and Dapino, M., 2010. *Applied Physics Letters* 96 012502.
- [37] Wun-Fogle, M., Restorff, J., and Clark, A., 2006. *IEEE Transactions on Magnetics* 42 3120–3122.
- [38] Armstrong, W. D., 2003. *Journal of Magnetism and Magnetic Materials* 263 208–219.
- [39] Jiles, D. C. and Atherton, D. L., 1986. *Journal of Magnetism and Magnetic Materials* 61 48–60.
- [40] Evans, P. G. and Dapino, M. J., 2010. Journal of Applied Physics 108 074517.
- [41] Deng, Z., Scheidler, J. J., Asnani, V. M., and Dapino, M. J., 2016. *Journal of Applied Physics* 120 243901.
- [42] Evans, P., 2009. "Nonlinear magnetomechanical modeling and characterization of Galfenol and system-level modeling of Galfenol-based transducers". PhD Thesis, The Ohio State University.
- [43] Atulasimha, J., Flatau, A. B., and Cullen, J. R., 2008. *Journal of Applied Physics* 103 014901.
- [44] Atulasimha, J., and Flatau, A. B., 2008. *Journal of Intelligent Systems and Structures* 19 1371–1381.
- [45] Clark, A. E., Restorff, J. B., Wun-Fogle, M., and Lograsso, T. A., 2000. *IEEE International* Toronto, Canada, April 9– 13, 2000.
- [46] Datta, S., Atulasimha, J., and Flatau, A. B., 2009. *Journal of Magnetism and Magnetic Materials* 321 4017–4031.
- [47] Clark, A. E., Wun-Fogle, M., Restorff, J. B., and Lograsso, T. A., 2002. *Material Transactions* 43 881–886.
- [48] Evans, P. G., and Dapino, M. J., 2008. *IEEE Transactions on Magnetics* 44 1711–1720.
- [49] Kellogg, R. A., Flatau, A. B., Clark, A. E., Wun-Fogle, M., and Lograsso, T. A., 2002. *Journal of Applied Physics* 91 7821